Journal of the Meteorological Society of Japan

## EARLY ONLINE RELEASE

This is a PDF of a manuscript that has been peer-reviewed and accepted for publication. As the article has not yet been formatted, copy edited or proofread, the final published version may be different from the early online release.



The DOI for this manuscript is
DOI:10.2151/jmsj.2020-065
J-STAGE Advance published date: August 28th, 2020

The final manuscript after publication will replace the preliminary version at the above DOI once it is available.

# Responses of Polar Mesocyclone Genesis to Topographic Forcing along the Eastern Coast of Eurasian Continent

**Kenta TAMURA**[1]

*Graduate School of Environmental Science*
*Hokkaido University, Sapporo, Japan*

**and**

**Tomonori SATO**

*Faculty of Environmental Earth Science*
*Hokkaido University, Sapporo, Japan*

December 20, 2019

-----------------------------------

1) Corresponding author: Kenta Tamura, Hokkaido University, North-10 West-5, Sapporo 060-0810, JAPAN.
Email: tamura_kenta@ees.hokudai.ac.jp
Tel: +81-11-706-2298

## Abstract

Polar mesocyclones (PMCs) occur frequently over the northern Sea of Japan. In this study, topographic effects on PMC genesis in this region were examined using long-term numerical simulations extending over 36 winter seasons. Sensitivity experiments showed that PMC genesis decreases in the part of the northern Sea of Japan when the mountain region at the eastern end of the Eurasian continent is removed. For example, the generation of PMCs over offshore west of Hokkaido decreases significantly when the mountain range is removed, whereas the generation of PMCs over the Strait of Tartary remains unchanged. According to composite analysis, this result can be attributed to the different responses of subregional oceanic surface wind to the removal of the mountains. In the experiment without mountains, cold air outbreaks from the continent blow directly over the Sea of Japan causing strong westerly winds over the offshore west of Hokkaido. Consequently, PMCs tend to make landfall earlier and before reaching maturity. The uniformly distributed westerly wind also has negative impact on PMC genesis because of weakened horizontal wind shear and meridional temperature gradient. In contrast, the low-level wind over the Strait of Tartary prior to PMC genesis is unaffected by the mountains and thus topographic effects are not required for PMC genesis in this region. These results indicate that the responses of PMCs to topographic forcing has a regional

variability.

**Keywords** polar mesocyclone; Sea of Japan; Strait of Tartary; topographic forcing; long-term numerical simulations

## 1. Introduction

Polar mesocyclones (PMCs) are mesoscale cyclones that develop over high-latitude oceans in the cold season. Intense meso-α-scale (200–1000 km) PMCs are called polar lows (Rasmussen and Turner 2003). PMCs occur frequently over reasonably warm oceans in association with outbreaks of cold continental air (Rasmussen and Turner 2003). PMCs often cause locally heavy snowfall and strong winds around coastal seas and land areas in the circumpolar region. Therefore, the genesis and development processes of PMCs have attracted considerable scientific attention, especially in the seas such as the Barents Sea (e.g., Rasmussen 1985), Labrador Sea (e.g., Mailhot et al. 1996), and Sea of Japan (e.g., Tsuboki and Wakahama 1992).

Several earlier case studies suggested that multiple mechanisms could contribute to PMC development. For example, baroclinic instability is essential during the initial stage of development of PMC (e.g., Reed and Duncan 1987), while conditional instability of the second kind and wind-induced surface heat exchange (WISHE) processes can help their rapid development (e.g., Rasmussen 1979; Emanuel and Rotunno 1989). An idealized numerical simulation revealed that the principal energy source for PMC development varies in accordance with synoptic-scale baroclinicity (Yanase and Niino 2007). The PMCs that develop under such different synoptic-scale conditions exhibit different cloud patterns. These earlier studies highlighted that PMCs can experience different formation and development processes and thus the role of environmental conditions can differ from case to case.

In addition to meteorological and oceanic effects, topographic effects can have a crucial role in PMC genesis. Over the Barents Sea, cold air outbreaks originating from the Arctic Sea can be split by the Svalbard islands, forming lower-tropospheric vorticity filaments that later grow into PMCs (Sergeev et al. 2018). The mountains located in the north of the Korean Peninsula can intensify a convergence zone over the southern Sea of Japan, along which frequent PMC genesis is observed (Watanabe et al. 2018). Despite the substantial impact of topographic effects on PMC genesis, previous discussions have tended to focus on case studies or idealized numerical experiments (e.g., Kristjánsson et al. 2011). Therefore, because the role of topographic effects on the genesis of various forms of PMC is not fully understood, the impact of topographic effects on the climatological features of PMCs also remains unexplored.

The frequency of occurrence of PMCs is very high over the northern Sea of Japan (Asai 1988), especially offshore west of Hokkaido (Fujiyoshi and Wakahama 1988). The horizontal scale of typical PMC in this region ranges from 200 km to 700 km (Tsuboki and Wakahama 1992). In this region, a PMC tends to be generated under strong horizontal wind shear caused by warm easterly wind and cold westerly wind associated with a synoptic-scale cyclone located to the east of the PMC (Ninomiya 1991; Ninomiya et al. 1993). This region of the Sea of Japan is surrounded by land (i.e., the Eurasian continent and Hokkaido) and areas of sea ice that can affect PMC genesis (e.g., Okabayashi and Satomi 1971;

Muramatsu 1975). The mountain range on the eastern edge of the Eurasian continent (i.e., the Sikhote-Alin mountain region) weakens the westerly wind over the Sea of Japan, establishing conditions suitable for PMC growth that allow PMCs to remain longer over the sea (Watanabe et al. 2017). In addition, the mountain range creates local (Ohtake et al. 2009) and synoptic-scale (Ninomiya 1991) horizontal temperature gradients in the lower troposphere which are likely to affect PMC genesis.

Although previous studies have highlighted that PMC generations over the offshore west of Hokkaido are affected by topography (e.g., Okabayashi and Satomi 1971; Muramatsu 1975; Watanabe et al. 2017), these studies intended to target the particular PMC cases. As described previously, the physical processes of PMC genesis differ on a case-by-case basis (Yanase and Niino 2007). In addition, due to the complexity of the effects of the topographic forcing, it is unclear how much of PMCs are affected by the suggested mechanisms. To examine the effects of the topographic forcing for such disturbances, it is useful to study how the disturbances respond to topography by numerical experiments with modified topography (e.g., Ohtake et al. 2009; Kristjansson et al, 2009, 2011, Watanabe et al. 2017). Therefore, it is necessary to clarify the possible roles of topographic effects on PMC genesis through the investigation of many PMC cases by using numerical experiments.

This study investigated the effects of the Sikhote-Alin mountain region on many different PMC cases in the offshore west of Hokkaido by the sensitivity experiments using modulated topography. We found a wide range of sensitivity of PMCs to topographic forcing, i.e., some

PMCs were highly sensitive to topographic effects, whereas others were less sensitive. The purpose of this study was to investigate the spatial and temporal variability of PMC genesis associated with topographic effects. We performed a long-term numerical experiment with realistic conditions in conjunction with sensitivity experiments. As we will introduce in section 3, the long-term sensitivity experiments succeeded in evaluation of the topographic impact on various types of PMCs geneses. Based on the experiments, we discriminated what types of PMCs are sensitive or not sensitive to the topographic forcing. The methods adopted in this study are described in section 2. In section 3, the results of the detection and tracking of PMCs are presented. Section 4 provides a discussion and our conclusions.

## 2. Data and methods

### *2.1 Numerical experiments*

We used the Weather Research and Forecasting (WRF) Model version 3.2.1 with the Advanced Research version of WRF (ARW) core (Skamarock et al. 2008). The model domain had 140 × 100 horizontal grid points with 20-km grid size and 32 vertical levels from the surface to the 50-hPa level (Fig. 1). With this horizontal grid size, we study PMCs whose horizontal scale is approximately larger than 100 km. This would reproduce majority of the PMCs generated in the study area because their diameter is typically larger than 100 km (e.g., Tsuboki and Wakahama 1992; Yanase et al. 2016). We used the following physics schemes as they can simulate well the mean and interannual variation of the precipitation around the Sea of Japan in snowy season (October to April) (Sato and Sugimoto 2013): the WRF Single Moment 6-class microphysical scheme (Hong et al. 2004), Grell 3D ensemble scheme (Grell and Devenyi 2002), rapid radiative transfer model for longwave parameterization (Mlawer et al. 1997), Dudhia scheme for shortwave radiation (Dudhia 1989), Mellor–Yamada–Nakanishi–Niino Level 2.5 planetary boundary layer scheme (Nakanishi and Niino 2004), and Noah land surface model (Chen and Dudhia, 2001）. The initial and boundary conditions were obtained from the Japanese 55-year Reanalysis (JRA-55) (Kobayashi et al, 2015), which provides six-hourly data with 1.25° resolution, and the NOAA 0.25° daily Optimum Interpolation Sea Surface Temperature and the distribution of sea ice dataset (OISST; Reynolds et al. 2007). The outer four rows from the lateral boundary were nudged to the forcing data. In this study, we did not use spectral nudging to consider that the topographic forcing may affect various scale atmospheric conditions such as upper-level flows.

We performed two types of WRF experiments that each covered 36 winter seasons (1 November 1981 to 31 March 2017). The experiments are started on 1 November and terminated on 31 March in each winter season. The first month (November) was regarded as a spin-up period and excluded from the analysis. The first experiment used realistic topography (hereafter, REAL, see Fig. 1a). In the second experiment, the Sikhote-Alin mountain region was removed (hereafter, NoMt; see Fig. 1b), i.e., we defined the mountainous topographic height is as greater than 100m and the topographic height was set to 100 m if the land elevation was greater than100 m. We analyzed the model output for the period between 1 December and 31 March. After performing the numerical experiments, we detected PMCs using the procedure introduced in the following section, and we compared the simulated PMCs to discuss the importance of topography on PMC genesis.

### *2.2 Detection of PMCs*

Although, previous studies have developed tracking algorithms to detect polar lows or PMCs (e.g., Yanase et al. 2016, Watanabe et al. 2016, Stoll et al. 2018), we developed a new tracking algorithm for detection of PMCs. To detect PMCs that include local disturbance, this algorithm does not require the threshold of the upper-level atmospheric conditions used in the previous studies. This enables us to analyze various types of PMCs as well as undeveloped PMC cases as discussed later. The workflow of the algorithm is as follows (Fig. 2). A center of low pressure is detected as the local minimum grid point of the 850-hPa geopotential height (Fig. 2b). On the grid point detected as the center of low pressure, if the relative vorticity at 850 hPa is greater than $1.0 \times 10^{-5}$ $s^{-1}$ and the center of low pressure appears over the sea, the low is designated as a cyclone and its movement is tracked. The threshold was determined as to most similarly produce the distribution of observed PMC (Fujiyoshi and Wakahama 1988). If stronger threshold (i.e., $1.0 \times 10^{-4}$ $s^{-1}$) was adopted, many PMCs generated near the coastal area were not detected. After one hour, if a center of low pressure is detected within 50 km of a previous center of low pressure, the low is regarded as the same cyclone (Fig. 2c). This tracking process is repeated for all cyclones generated over the sea. The above procedure could also detect synoptic-scale cyclones (i.e., extratropical cyclones) whose horizontal size is much greater than a PMC. To remove synoptic-scale cyclones, the following procedure was incorporated. The 850-hPa geopotential height field derived from the original 20-km mesh WRF output (Fig. 2a) is smoothed to a 100-km mesh grid (Fig. 2d), and centers of low pressure are detected using the smoothed field (Fig. 2e). Eventually, the absolute location of the center within a 100-km mesh grid is determined by using the original 20-km mesh data (850-hPa geopotential height minima) so that the locations of the low pressure center are consistent before and after smoothing (Fig. 2e). In this attempt, only large-scale cyclones (diameter is over ~300km) are detected (Fig. 2f), which contrasts with the lows detected without smoothing (i.e., 20-km mesh grid) that include all cyclone features (Fig. 2c). The low pressures detected in both attempts are regarded as synoptic-scale cyclones (Fig. 2g) that were excluded from further analysis. At least, the diameter of the remaining low pressures is less than ~300 km at the first detected time. The diameter of PMC may exceed 300 km during the tracking. In such a case, the low pressure has been kept assigned as a PMC because the point of the first detections are different between before and after smoothing. Consequently, these lows are regarded as PMCs that were included in the analysis if they continuously satisfied the above requirements for at least 12 hours (unless otherwise stated).

## 3. Results

### *3.1 Number of PMCs*

The distribution of PMC genesis is shown in Fig. 3. In the REAL experiment, PMCs occur frequently over the area offshore west of Hokkaido and over the Strait of Tartary (Fig. 3a). This distribution pattern is similar to that of polar lows detected using reanalysis data (Yanase et al. 2016). However, the number is relatively higher in this study because we intended to include smaller-scale PMCs by using finer mesh data and weaker thresholds. The number of generated PMCs is lower in the NoMt experiment in comparison with the REAL experiment, especially over the western coastal sea of Hokkaido (Fig. 3b). This result indicates that the Sikhote-Alin mountain region strongly enhances PMC genesis over the study area.

The seasonal variation in the number of PMCs generated in the area offshore west of Hokkaido (43°–49°N, 138°–142°E) is shown in Fig. 4. In the REAL experiment, the number of generated PMCs is lowest in December, reaches a peak in January, and then falls through February and March, which is consistent with satellite data analysis (Fujiyoshi and Wakahama 1988). In the NoMt experiment, the number of PMCs generated in January dramatically decreases to 55% of REAL experiment followed by December (60%) and February (64%), whereas there is a weak decrease in March (77%). Therefore, the contribution of the mountain region to PMC genesis varies depending on the month. Furthermore, this implies that PMCs could be classified into two groups: those sensitive to topographic effects and those less sensitive. Among the various PMCs occurring in each month, the majority in January seems to require topographic effects in the genesis stage.

The direction of movement of PMCs generated in the area offshore west of Hokkaido varies depending on the synoptic-scale environments prevailing at the time of their occurrence. A PMC moves southward when an extratropical cyclone is located to its east, whereas it moves eastward in association with an eastward-migrating upper-level trough (Yanase et al. 2016). The number of PMCs moving in each of the four main cardinal directions is shown in Fig. 5. Here, the direction of movement is defined as the orientation of the line connecting the points of PMC occurrence and disappearance. The dominant directions of movement in the REAL experiment are southward and eastward. Southward-moving PMCs occur more frequently in January than in the other months. In the NoMt experiment, the number of southward-moving PMCs is reduced in comparison with REAL, while that of eastward-moving PMCs is less reduced.

*3.2 Distribution of PMC genesis*

The NoMt experiment indicates that PMCs generated in January are strongly affected by the Sikhote-Alin mountain region (Fig. 4) if the predominant direction of movement of the PMCs is southward (Fig. 5b). The spatial distribution of PMC genesis in January is shown in Fig. 6. The number of southward-moving PMCs generated along the offshore area west of Hokkaido and over the Strait of Tartary is high (Fig. 6a), while the genesis of eastward-moving PMCs is scattered more widely (Fig. 6b). The difference in the distribution of southward- and eastward-moving PMCs between the NoMt and REAL experiments (NoMt − REAL) is shown in Fig. 6e and 6f, respectively. It can be seen that the effect of the Sikhote-Alin mountain region on the PMC genesis is different between the Strait of Tartary and offshore west of Hokkaido. In the NoMt experiment, a few southward-moving PMCs are generated south of 46°N (Fig. 6c) and the difference in the number of southward-moving PMCs genesis is large (Fig. 6e). By removing the mountains, the number of eastward-moving PMC genesis is reduced over the south of 46°N and increase over the north of 46°N (Fig. 6f). This result suggests that the characteristics of PMCs are different between the Strait of Tartary and offshore west of Hokkaido. In addition, eastward-moving PMC frequently occurs near the west coast of Hokkaido (140°E–142°E) only in January (Supplement 1) and its number is substantially decreased due to the removal of the mountain range (Supplement 2).

Considering the different sensitivity of PMCs to topographic forcing within the study region (Fig. 6), we defined two subregions: offshore west of Hokkaido (43°–46°N, 138°–142°E) and the Strait of Tartary (46°–49°N, 138°–142°E). In the following, PMCs generated in the offshore west of Hokkaido are referred to as WH-PMCs, PMCs generated in the Strait of Tartary are referred to as ST-PMCs. The monthly variation of the number of PMCs generated in the two subregions is shown in Fig. 7. In the offshore west of Hokkaido, PMCs occur most frequently in January (Fig. 7a). In the NoMt experiment, the number of WH-PMCs (both southward- and eastward-moving systems) in January decreases to less than 50% of the REAL experiment. Similar reductions in WH-PMCs are found for southward-moving systems in each month; however, interestingly, the number of eastward-moving systems does not change in December, February, and March. In January, the number of generated ST-PMCs is lower in comparison with WH-PMCs, and the difference between the REAL and NoMT experiments is small (Fig. 7b). Comparing the number of PMC genesis between the subregions and months, PMCs generated over the offshore west of Hokkaido in January seem most sensitive to the mountain regions. The reasons for the different sensitivity of the PMCs are discussed in the following sections.

*3.3 Atmospheric conditions*

Based on composite analysis, the synoptic-scale atmospheric patterns leading to the different sensitivity between the two subregions are highlighted. The composite field of the 500- and 850-hPa geopotential height for the time of PMC genesis in January is shown in Fig. 8. At the time of WH-PMC genesis, a synoptic-scale lower-tropospheric cyclone appears over the Kamchatka Peninsula as a part of Aleutian low (Fig. 8c). The synoptic-scale pressure patterns are similar between southward-moving (blue contours) and eastward-moving (red contours) PMCs (Fig. 8a and 8c). For ST-PMCs, the synoptic-scale pressure patterns are different between the two directions of movement (Fig. 8b and 8d). For southward-moving ST-PMCs, the synoptic-scale pressure pattern resembles that of WH-PMCs (Fig. 8b and 8d). However, the generation of eastward-moving ST-PMCs is not associated with Aleutian low (Fig. 8d). Locations of upper-level low pressure vary with PMCs depending on the moving directions and generated regions. For southward-moving PMC the upper-level low tends to collocate with or locate to the north of the surface low, and for eastward-moving PMC it locates to the northwest of the surface low (Fig. 8a and 8b). Presumably, southward-moving PMCs are developed through the active convection induced by the upper-level cold troughs while eastward-moving PMCs develop through baroclinic interaction with the upper-level troughs (Yanase et al. 2016). It should be noted that Fig. 8 does not show clearly the upper-level synoptic-scale atmospheric conditions at the developmental stage because it shows the composite fields at the PMCs genesis. Focusing on the PMC tracks, most southward-moving PMCs initially move southwestward and then move southeastward, apparently affected by the cyclonic circulation associated with Aleutian low (Fig. 8c and 8d). Eastward-moving PMCs are more likely to follow an eastward-moving mid-tropospheric trough. The moving direction is, however, not unique even if synoptic-scale atmospheric condition during PMCs genesis is similar as shown in Fig. 8c. The PMC movement could vary according to the post-genesis synoptic circulation changes, such as caused by the transition of Aleutian low and other synoptic-scale low pressure.

Figure 9 displays temporal and vertical variations of relative vorticity in the PMC.

Southward-moving WH-PMC has intense vorticity comparing to the others (Fig. 9a). The relative vorticity of eastward-moving PMCs became weak within 12 hours after the genesis, suggesting the earlier landfall than southward-moving PMCs (Fig. 9c and 9d). PMCs are characterized as a shallow system at their early developmental stage and the strong vorticity extends vertically along with the development of the PMCs. Since we focus on the PMCs genesis, we analyze the lower-level atmospheric conditions hereafter.

The composite field of potential temperature and wind at 850 hPa 12 hours before PMC genesis in the REAL experiment is shown in Fig. 10. The temperature gradient from northwest to southeast across the domain suggests the occurrence of cold air outbreaks (Fig. 10a–c). A part of the cold air outbreaks passes across the southern part of the Sikhote-Alin mountain region, where the elevation is relatively low and then causes northwesterly wind over the Sea of Japan (Fig. 1a). In addition, northerly wind blowing from the Strait of Tartary is found for WH-PMCs cases (Fig. 10a and 10c). These wind systems can form horizontal wind shear over the offshore west of Hokkaido. In the case of the ST-PMCs moving eastward, the low-level wind pattern is different from other PMCs, with southwesterly winds and higher potential temperature at 850-hPa over the Sea of Japan (Fig. 10d). It seems that the cold air outbreaks do not affect the genesis of the eastward-moving ST-PMC.

The difference in 850-hPa winds between the NoMt and REAL experiments (NoMt − REAL) is presented in Fig. 11 to investigate how the Sikhote-Alin mountain region might modulate the lower-tropospheric wind. Here, the reference time for the composite analysis is common for both experiments, i.e., 12 hours before PMC genesis in the REAL experiment. In the NoMt experiment, in comparison with the REAL experiment, the westerly wind component is stronger, and the potential temperature is lower over the offshore west of Hokkaido (Fig. 11). In addition, the northerly wind over the Strait of Tartary is slightly weak and the potential temperature is a little higher in NoMt experiment, which are the common circulation changes for many PMC types as found in Fig. 11a-c. These differences are not clear in the case of eastward-moving ST-PMCs (Fig. 11d).

Figure 12 shows the potential temperature along the cross sections A–A', B–B', and C–C' (see Fig. 11). When PMC genesis occurs in offshore west of Hokkaido, a meridional potential temperature gradient around 46°N is strong for southward-moving PMCs but it weakens in NoMt experiment (Fig. 12a). In the case of southward-moving WH-PMC, the area of strong zonal potential temperature gradient on 138°E shifts eastward (Fig. 12c). Similarly, the area of large potential temperature gradient around 47°N for southward-moving ST-PMCs retreats northward (Fig. 12b). On the Strait of Tartary (Fig. 12d), the potential temperature for ST-PMCs case slightly increases in NoMt experiment. These suggest that, after the removal of the Sikhote-Alin mountain region, cold air outbreaks from the continent tend to blow directly over the Sea of Japan, which consequently weakens the cold advection from the Strait of Tartary. Based on this evidence, it is speculated that the changes in wind and temperature in the lower-troposphere are fundamental to the understanding of the diverse response of PMC genesis to topographic forcing.

*3.4 Characteristics of PMCs*

The Sikhote-Alin mountain region forms the horizontal wind shear over the Sea of Japan (Fig. 10a and 10c), which is likely to affect the probability of PMC genesis. We found that the mountain reduces the zonal wind speed over the western part of the Sea of Japan (Fig. 11a–11c). Furthermore, the mountain region has a role to form horizontal temperature gradients over the offshore west of Hokkaido (Fig. 12). To discuss how they affect the PMC genesis, longitudinal distribution of PMC genesis is investigated. This analysis here includes short-lived PMCs to ensure consideration of both assigned (i.e. developed) and unassigned (i.e. undeveloped) PMCs. To account for short-lived mesocyclones, we relaxed the detection requirement by shortening the minimum lifespan from original twelve hours (See section 2.2) to six hours. The longitudinal distributions of the locations of PMC genesis in the two experiments are shown in Fig. 13. The number of WH-PMCs generated near the Eurasian continent (138°E to 140°E) in the REAL experiment (78 counts per 36 winters) is reduced in the NoMt experiment (27 counts), while the reduction is relatively minor (81 and 50 counts for REAL and NoMt respectively) near Hokkaido (140°E to 142°E) (Fig. 13a). In contrast, the number of ST-PMCs does not differ between the two experiments (Fig. 13b). These results suggest the Sikhote-Alin mountain region can form horizontal wind shear in the downwind vicinity, which enhance PMC genesis over the western part of the western offshore of Hokkaido, while the impact is weaker over the eastern part (i.e., near the

Hokkaido).

A strong westerly wind over the ocean is likely to accelerate the speed of movement of PMCs, promoting landfall of early stage PMCs on the islands (Watanabe et al. 2017). The duration between PMC genesis and landfall is summarized in Fig. 14. The mean duration of WH-PMCs in the NoMt experiment (6.0 h) is significantly shorter (Welch's t-test, $p = 0.008$) than in the REAL experiment (9.4 h). ST-PMCs do not exhibit significant changes in their lifespan. This result indicates that without Sikhote-Alin mountain region, WH-PMC's landfall on Hokkaido occurs earlier, whereas ST-PMC's landfall on Hokkaido or Sakhalin remain unchanged. These characteristics are found only in January (Supplement 3) because the southward- and eastward-moving PMCs frequently occur near the west coast of Hokkaido only in January (Supplement 1). Without mountains, the rate of landfall for WH-PMCs (ST-PMCs) increases from 52% to 61% (43% to 49%). The Sikhote-Alin mountain region weakens the westerly wind (Fig. 11), which allows PMCs to remain longer over the ocean. Through analysis of many PMC cases, our study confirms that the effect of the Sikhote-Alin mountain region in modulating the environmental winds and the lifespan of generated PMCs is robust in the offshore west of Hokkaido but not in the Strait of Tartary.

## 4. Discussion and Conclusions

In this study, we performed long-term numerical experiments to investigate the effects of topography (i.e., the Sikhote-Alin mountain region) on PMCs generated over the northern Sea of Japan. The comparison of PMCs between REAL experiment and NoMt experiment is summarized in table 1. We found that the effects of the Sikhote-Alin mountain region on PMCs vary depending on slight differences in genesis location and month. Among the many PMCs investigated, those generated over the offshore west of Hokkaido are most sensitive to topographic effects, while those generated over the Strait of Tartary are less sensitive. The difference in sensitivity is attributable to local modulation of the topographically induced oceanic winds.

During WH-PMC genesis, the horizontal wind shear over the offshore west of Hokkaido is formed because of two wind systems: a northwesterly wind from the continent and a northerly wind from the Strait of Tartary (Fig. 10a and 10c). This horizontal wind shear is likely induced by cyclonic circulation related to the passage of synoptic-scale lower-tropospheric cyclones (Fig. 8a and 8c), similar to the case study by Ninomiya (1991). The northwesterly wind over the Sea of Japan originates from the air mass passing across the Sikhote-Alin mountain region. Therefore, the wind shear is very sensitive to the local topography. Conversely, for ST-PMC genesis, northerly wind from the Strait of Tartary is weak (Fig. 10b and 10d) because the cyclonic circulation of Aleutian low does not reach the Strait of Tartary (Fig. 8d).

The area of intensified westerly wind in the NoMt experiment (around 46°N) corresponds to the boundary between the northerly and northwesterly wind in the REAL experiment (Figs. 10 and 11). By removing the Sikhote-Alin mountain region, the westerly wind from the continent blows directly over the Sea of Japan. Consequently, the westerly wind over the offshore west of Hokkaido becomes horizontally uniform and wind shear becomes negligibly weak, which discourages WH-PMCs genesis. This wind shear shifts to the Strait of Tartary (Fig. 11a and 11b) and may cause northward shift of PMC genesis. In addition, even though enhanced westerly wind causes strong surface fluxes from the sea after the removal of the mountain range, the equivalent potential temperature over the offshore west of Hokkaido is decreased as a result of the dry and cold air inflow from the continent (not shown). The resultant stable condition may suppress the PMC genesis. However, in eastward-moving ST-PMCs, the wind and temperature fields do not vary by removing the Sikhote-Alin mountain region (Fig. 11d). Therefore, the occurrence of the eastward-moving ST-PMCs may not require lower-level wind shear. This PMC type could develop from baroclinic instability with an upper-level trough passage (Yanase et al. 2016).

Over the offshore west of Hokkaido, the cold air outbreaks from the Eurasian continent helps form zonal temperature gradient (Fig. 10 and 12c). Over the Strait of Tartary, meridional temperature gradient is intensified by the northerly wind, especially in the case of southward-moving PMC (Fig. 10 and 12a-b). Over the offshore west of Hokkaido, removal of the mountain range shifts the high zonal temperature gradient zone eastward, leading to the eastward shift of the PMC genesis and thereby more landfall before the PMC development. Therefore, the number of WH-PMCs is decreased. Furthermore, northward retreat of the high meridional temperature gradient zone due to the removal of the mountain also causes northward shift of PMC genesis. Due to this shift in genesis location, some WH-PMCs in the REAL experiment could be counted as ST-PMC in the NoMt experiment.

PMC (and short-lived mesocyclone) genesis over the offshore west of Hokkaido (138°–140°E) is reduced by the removal of the Sikhote-Alin mountain region (Fig. 13a). However, the mountain effect on the genesis of the PMC is weak for coastal offshore areas (140°–142°E). Along the west coast of Hokkaido, local cold air outbreaks often occur from Hokkaido toward the Sea of Japan. This produces horizontal wind shear over the sea, establishing conditions favorable for PMC genesis (e.g., Okabayashi and Satomi 1971; Muramatsu et al. 1975; Tsuboki and Wakahama 1992). Therefore, it is speculated that the likelihood of PMCs genesis over the coastal region remains similar, even after the removal of the Sikhote-Alin mountain region.

Among the many PMCs generated in January that moved southward, PMC genesis decreases only over the offshore west of Hokkaido (Fig. 7a and 7b). Without the Sikhote-Alin mountain region, WH-PMCs tend to make early landfall, while ST-PMCs do not (Fig. 14). Moreover, the lower-tropospheric westerly to the south of the Strait of Tartary (around 46°N) becomes stronger, while little change was detected over the Strait of Tartary (north of 46°N) (Fig. 11b and 11d). In the NoMt experiment, WH-PMCs are affected by the westerly wind in their genesis stage because they occur under the condition of the westerly wind enhanced by removal of the mountains. In contrast, ST-PMCs are not affected by the westerly wind during their genesis stage because their genesis location is to the north of the strong westerly zone. When ST-PMCs move southward, they enter the strong westerly zone after they grow. Since PMCs are characterized as a shallow system at their early developmental stage (Fig. 9), lower-tropospheric wind might only affect the development of early-stage PMCs but not the latter stage. For WH-PMCs, intensified low-level westerly due to the mountain removal pushes early-stage PMCs eastward and enhances landfall on Hokkaido, and hence the number is reduced. On the other hand, the southward-moving ST-PMCs typically migrate offshore west of Hokkaido at their mature stage. Because of the vertical extending of vorticity along with the development of PMCs (Fig. 9), they are less affected by the lower-level wind. For eastward-moving ST-PMCs, the baroclinic instability is likely to be a primary development mechanism (Yanase et al., 2016), the upper-level synoptic environment is more crucial than lower-level circulation (Fig. 8b). Since the mountain range hardly disturbs the upper-level fields, eastward ST-PMCs are not affected by the removal of the mountain range. Hence, ST-PMCs are not sensitive to the effects of the Sikhote-Alin mountain region. In addition, sea ice extends to the northern part of the Strait of Tartary in January (Fig. 1). Near the ice edge, low-level baroclinicity stimulates the development of PMCs (Mailhot et al. 1996). Hence, ST-PMC genesis is likely affected more strongly by sea ice than by the Sikhote-Alin mountain region.

With regard to modulation of the lower-tropospheric environment and thus PMC genesis, this study clarified that the effect of the Sikhote-Alin mountain region is manifest in two major ways: intensified horizontal wind shear and weakened westerly wind. These effects are likely to enhance PMC genesis over the offshore west of Hokkaido. Moreover, we found that PMC sensitivity to the Sikhote-Alin mountain region varies with the location of PMC genesis, i.e., PMCs generated over the offshore west of Hokkaido are very sensitive, whereas those generated over the Strait of Tartary are insensitive. In order to investigate the sensitivity of PMCs to the mountain range, we performed an additional experiment in which the height of the mountains was halved (hereafter, HalfMt). Figure 15 compares the number of PMC genesis in each experiment. For WH-PMC, the number of PMCs decreases sharply in HalfMt experiment exhibiting the similar magnitude of reduction as in NoMt experiment, whereas the number of ST-PMCs remain almost unchanged (Fig. 15). This result indicates that the effect of the topography on PMCs vary locally.

Through the long-term numerical experiments, we confirmed that, in a climatology sense, WH-PMC genesis is sensitive to the topography. Since this study considers many PMCs, the sensitivity here means the tendency of behavior for PMC population. Given that expected response of PMC to mountain varies for each case, probably depending on the background synoptic patterns, the statistical approach like this study is useful to comprehensively understand the characteristics of PMC in the studied area.

In addition to the orographic effects, SST has known to affect the development of PMCs. PMC is likely to be modulated by variability of local sea surface conditions (e.g., Kolstad and Bracegirdle 2017). Furthermore, variations in SST and sea ice distribution can modulate the pattern and frequency of PMC genesis at various timescales, e.g., interannual to decadal. To clarify the trend of PMCs within such timescales, it will be necessary to analyze many PMC examples using long-term high-resolution numerical simulations that have recently become possible. It is also important to consider the effect of air-sea interaction. The numerical experiment in this study was conducted by an atmospheric model which does not predict oceanic response to modified atmospheric circulation. This offline ocean setting might underestimate the reduction of PMC genesis due to the removal of mountains. The accelerated low-level westerly and intensified cold air outbreaks in NoMt experiment enhance heat fluxes from the ocean and, consequently, could decrease SST (Kawamura and Wu 1998). The formation of PMC could be further reduced over the colder SST (Watanabe et al. 2017) in comparison to our NoMt experiment. To examine the role of air-sea interaction, future studies require a coupled model experiment with sufficient high spatial resolution and with better ability in simulating planetary boundary layer processes and mesoscale convection.

## Acknowledgments

This work was supported by the Arctic Challenge for Sustainability (ArCS) Project funded by MEXT (Japan) and JSPS KAKENHI Grant 19H05697 and 19H05668 funded by the Japan Society for the Promotion of Science (JSPS). The JRA-55 dataset was provided by the JMA. The OISST dataset was provided by NOAA (https:// www.ncdc.noaa.gov/oisst/). We thank James Buxton MSc from Edanz Group (www.edanzediting.com./ac) for editing a draft of this manuscript.

## References

Asai, T., 1988: Mesoscale features of heavy snowfalls in Japan Sea coastal regions of Japan. *Tenki*, **35**, 156−161, (in Japanese).

Chen, F., Dudhia J, 2001: Coupling an advanced land surface hydrology model with the Penn State-NCAR MM5 Modeling System. Part I: model implementation and sensitivity. *Mon Wea Rev.*, **129**, 569–585, doi: 10.1175/1520-0493(2001)129<0569:CAALSH> 2.0.CO;2

Dudhia, J., 1989: Numerical study of convection observed during the winter monsoon experiment using a mesoscale two-dimensional model. *J. Atmos. Sci*., **46**, 3077−3107, doi:10.1175/1520-0469(1989)046<3077:NSOCOD>2.0.CO;2.

Emanuel, K. A., and R. Rotunno, 1989: Polar lows as arctic hurricanes. *Tellus*, **41A**, 1–17, doi:10.1111/j.1600-0870.1989.tb00362.x.

Fujiyoshi, Y., K. Tsuboki, H. Konishi and G. Wakahama, 1988: Doppler radar observation of convergence band cloud formed on the west coast of Hokkaido Island (I): warm frontal type. *Tenki*, **35**, 427−439, (in Japanese).

Grell, G. A., and D. Devenyi, 2002: A generalized approach to parameterizing convection combining ensemble and data assimilation techniques. *Geophys. Res. Lett.*, **29**, 1693, doi:10.1029/2002GL015311.

Hong, S. Y., J. Dudhia, and S. H. Chen, 2004: A revised approach to ice microphysical processes for the bulk parameterization of clouds and precipitation. *Mon. Wea. Rev*., **132**, 103−120, doi:10.1175/1520-0493(2004)132<0103:ARATIM>2.0.CO;2.

Kobayashi, S., and Coauthors, 2015: The JRA-55 reanalysis: General specifications and basic characteristics. *J. Meteor. Soc. Japan*, **93**, 5–48, doi:10.2151/jmsj.2015-001.

Kolstad, E.W., and Bracegirdle, T.J, 2017: Sensitivity of an Apparently Hurricane-like Polar Low to Sea-surface Temperature. *Q. J. R. Meteorol. Soc.*, **143**, 966−973, doi:10.1002/qj.2980.

Kawamura, H., and P. Wu, 1998: Formation mechanism of Japan Sea Proper Water in the flux center off Vladivostok. *J. Geophys. Res.*, **103**, 21611-21622.

Kristjánsson, J. E., S. Thorsteinsson, and B. Røsting, 2009: Phase-locking of a rapidly developing extratropical cyclone by Greenland's orography. *Q. J. R. Meteorol. Soc.*, **135**, 1986–1998, doi:10.1002/qj.497.

------, S. Thorsteinsson, E. W. Kolstad, and A. M. Blechschmidt, 2011: Orographic influence of east Greenland on a polar low over the Denmark Strait. *Q. J. R. Meteorol. Soc.*, **137**, 1773–1789, doi:10.1002/qj.831.

Mailhot, J., D. Hanley, B. Bilodeau, and O. Hertzman, 1996: A numerical case study of a polar low in the Labrador Sea. *Tellus*, **48A**, 383−402, doi:10.3402/tellusa.v48i3.12067.

Muramatsu, T., S. Ogura and N. Kobayashi, 1975: The heavy snowfall arisen from small scale cyclone on the west coast of Hokkaido Island. *Tenki*, **22**, 369–379, (in Japanese).

Mlawer, E. J., S. J. Taubman, P. D. Brown, M. J. Iacono, and S. A. Clough, 1997: Radiative transfer for inhomogeneous atmosphere: RRTM, avalidated correlated-k model for the longwave. *J. Geophys. Res.*, **102(D14)**, 16,663–16,682, doi:10.1029/97JD00237.

Nakanishi, M., and H. Niino, 2004: An improved Mellor-Yamada level-3 model with condensation physics: Its design and verification. *Bound.-Layer Meteor.*, **112**, 1−31, doi:10.1007/s10546-005-9030-8.

Ninomiya, K., 1991: Polar low development over the east coast of the Asian continent on 9–11 December 1985. *J. Meteor. Soc. Japan*, **69**, 669–685, doi:10.2151/jmsj1965.69.6_669.

------, K. Wakahara, and H. Ohkubo, 1993: Meso-α-scale low development over the northeastern Japan Sea under the influence of a parent large-scale low and a cold vortex aloft. *J. Meteor. Soc. Japan*, **71**, 73–91, doi:10.2151/jmsj1965.71.1_73.

Ohtake, H., M. Kawashima, and Y. Fujiyoshi, 2009: The formation mechanism of a thick cloud band over the northern part of the Sea of Japan during cold air outbreaks. *J. Meteor. Soc. Japan*, **87**, 289–306, doi:10.2151/jmsj.87.289.

Okabayashi, T. and M. Satomi, 1971: A study on thesnowfall and its original clouds by meteorological radar and satellite (part I). *Tenki*, **18**, 573–581, (in Japanese).

Rasmussen, E., 1979: The polar low as an extratropical CISK disturbance. *Q. J. R. Meteorol. Soc.*, **105**, 531–549, doi:10.1002/qj.49710544504.

------, 1985: A case study of a polar low development over the Barents Sea. *Tellus*, **37A**, 407–418, doi:10.3402/tellusa.v37i5.11685.

------, and J. Turner, 2003: *Polar Lows*. Cambridge University Press, 612 pp.

Reed, R. J., and C. N. Duncan, 1987: Baroclinic instability as a mechanism for the serial development of polar lows: A case study. *Tellus*, **39A**, 376–384, doi:10.1111/j.1600–0870.1987.tb00314.x.

Reynolds, R., T. Smith, C. Liu, D. Chelton, K. Casey, and M. Schlax, 2007: Daily high-resolution-blended analyses for sea surface temperature. *J. Climate*, **20**, 5473–5496, doi:10.1175/2007JCLI1824.1.

Sato, T., and S. Sugimoto, 2013: A numerical experiment on the influence of the interannual variation of sea surface temperature on terrestrial precipitation in northern Japan during the cold season. *Water Resour. Res.*, **49**, 7763–7777, doi:10.1002/2012WR013206.

Sergeev, D., I. A. Renfrew, T. Spengler, 2018: Modification of Polar Low Development by Orography and Sea Ice. *Mon. Wea. Rev.*, **146**, 3325–3341, doi:10.1175/MWR-D-18-

0086.1.

Skamarock, W. C., J. B. Klemp, J. Dudhia, D. M. Barker, M. G. Duda, X.-Y. Huang, W. Wang, and J. G. Powers, 2008: A description of the Advanced Research WRF version 3. Tech. Note NCAR/TN-475+STR, Natl. Cent. for Atmos. Res., Boulder, Colo, 113 pp.

Stoll, P. J., Graversen, R. G., Noer, G., and Hodges, K., 2018: An objective global climatology of polar lows based on reanalysis data. *Q. J. R. Meteorol. Soc.*, **144**, 2099–2117, doi: 10.1002/qj.3309.

Tsuboki, K., and G. Wakahama, 1992: Mesoscale cyclogenesis in winter monsoon air streams: Quasi-geostrophic baroclinic instability as a mechanism of the cyclogenesis off the west coast of Hokkaido Island. Japan. *J. Meteor. Soc. Japan*, **70**, 77–93, doi:10.2151/jmsj1965.70.1_77.

Watanabe, S. I., H. Niino, and W. Yanase, 2017: Structure and environment of polar mesocyclones over the northeastern part of the Sea of Japan. *Mon. Wea. Rev.*, **145**, 2217–2233, doi:10.1175/MWR-D-16-0342.1.

------, ------, and ------, 2018: Composite analysis of polar mesocyclones over the western part of the Sea of Japan. *Mon. Wea. Rev.*, **146**, 985–1004, doi:10.1175/MWR-D-17-0107.1.

Yanase, W., and H. Niino, 2007: Dependence of polar low development on baroclinicity and physical processes: An idealized high-resolution numerical experiment. *J. Atmos. Sci.*, **64**, 3044–3067, doi:10.1175/JAS4001.1.

------, ------, S. I. Watanabe, K. Hodges, M. Zahn, T. Spengler, and I. A. Gurvich, 2016: Climatology of polar lows over the Sea of Japan using the JRA-55 reanalysis. *J. Climate*, **29**, 419–437, doi:10.1175/JCLI-D-15-0291.1.

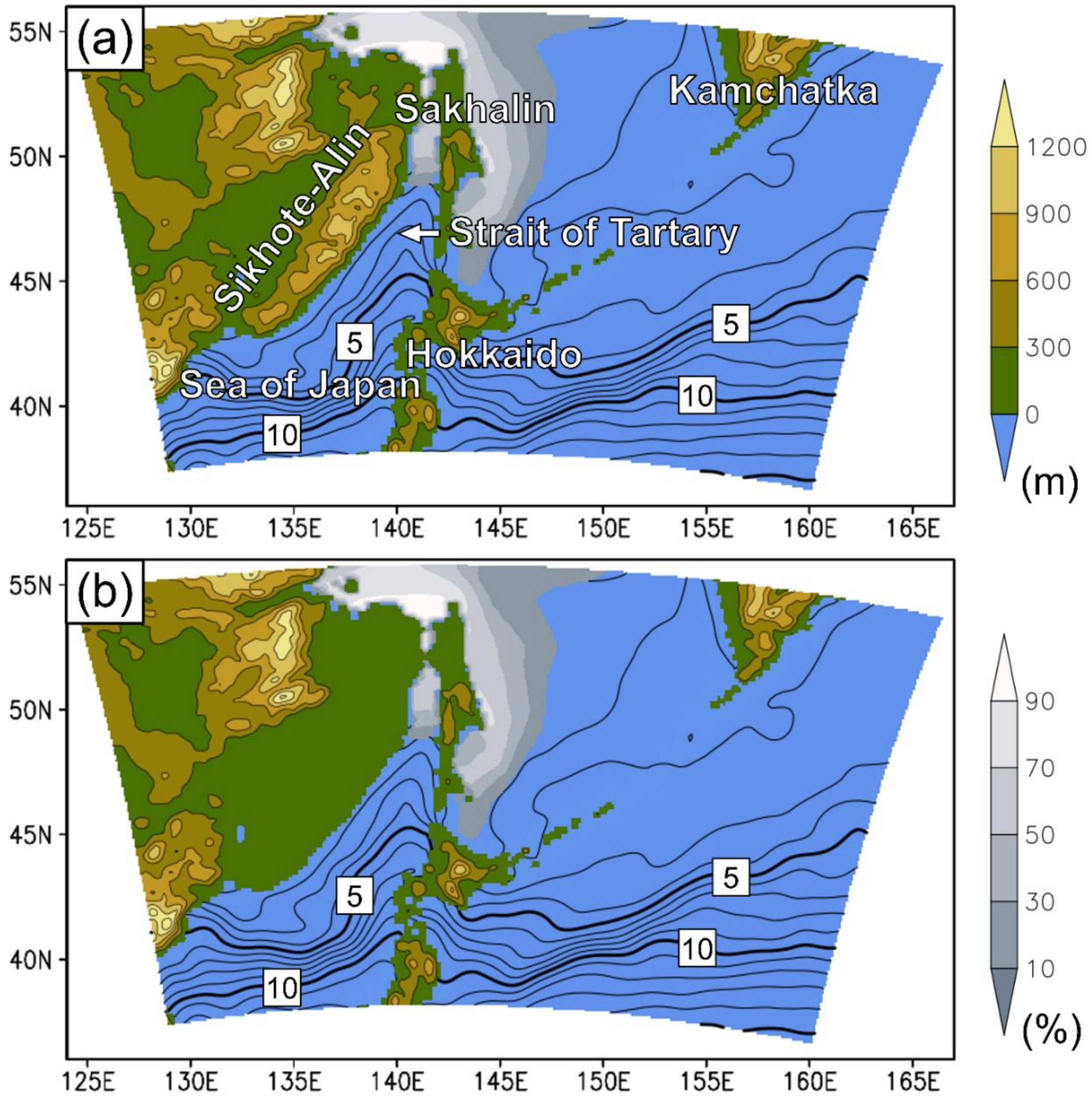


Fig. 1 Topography (color; m), January mean SST (contours; interval 1°C), and distribution of sea ice concentration (gray shading, %) around Hokkaido in the numerical simulations. Topography shown in (a) was used for the REAL experiment, while that shown in (b) was used for the NoMt experiment.

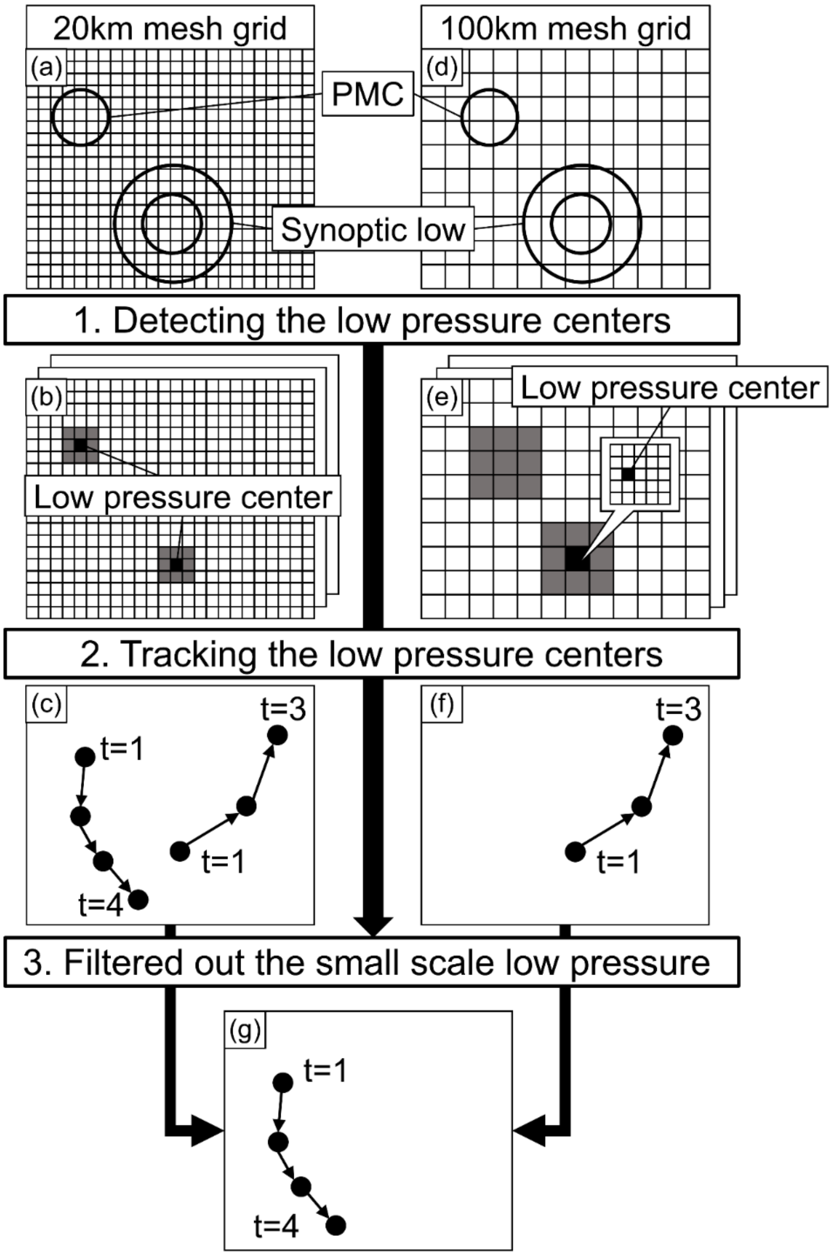


Fig. 2 Schematic of the workflow of the PMC detection algorithm. (a) Original grid (20-km mesh grid) and (d) smoothed grid (100-km mesh grid). (b) and (e) Gray-filled grids indicate the search area validating whether there is a local minimum 850-hPa geopotential height within 3×3 grids. Black-filled grids indicate detected centers of low pressure. (c) and (f) Detected centers of low pressure and their tracks. (g) Track of a detected PMC. Full details are provided in the text.

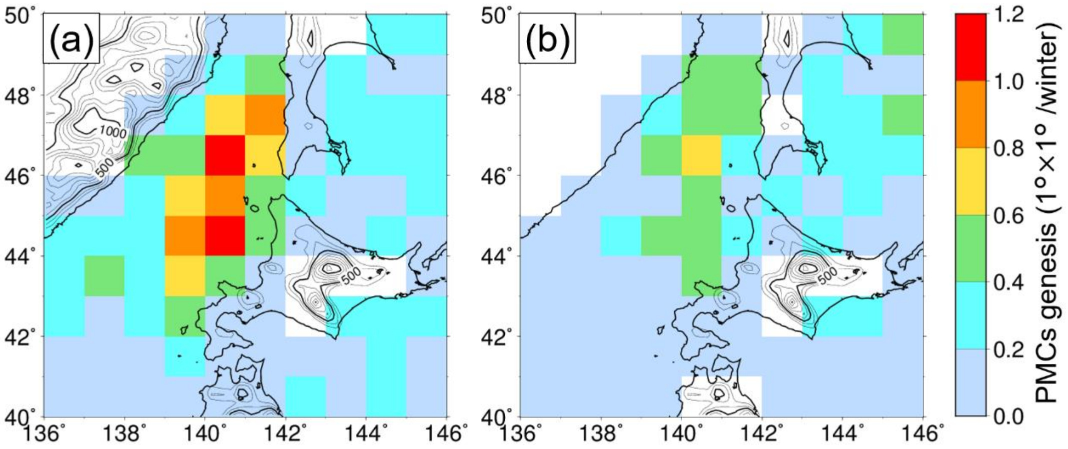


Fig. 3 Distribution of PMC genesis over the 36 winter seasons between December 1981 and March 2017: (a) REAL experiment and (b) NoMt experiment. Colors indicate the number of PMCs generated within each 1° × 1° box (/winter).

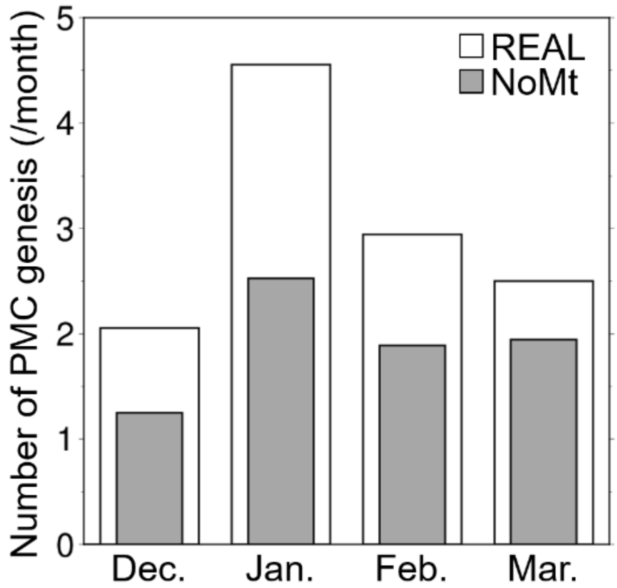


Fig. 4 Number of PMCs generated within the analysis domain (43°–49°N, 138°−142°E) in each month. White (gray) bar indicates REAL (NoMt) experiment.

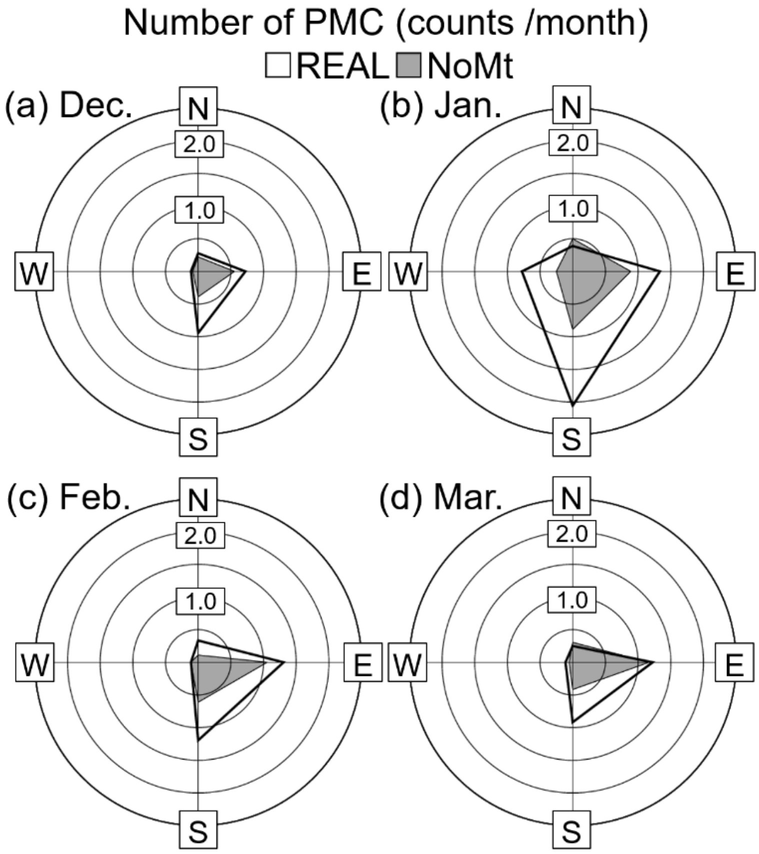


Fig. 5 Number of PMCs moving in each of the four main cardinal directions. Black line (gray shading) indicates PMCs in the REAL (NoMt) experiment.

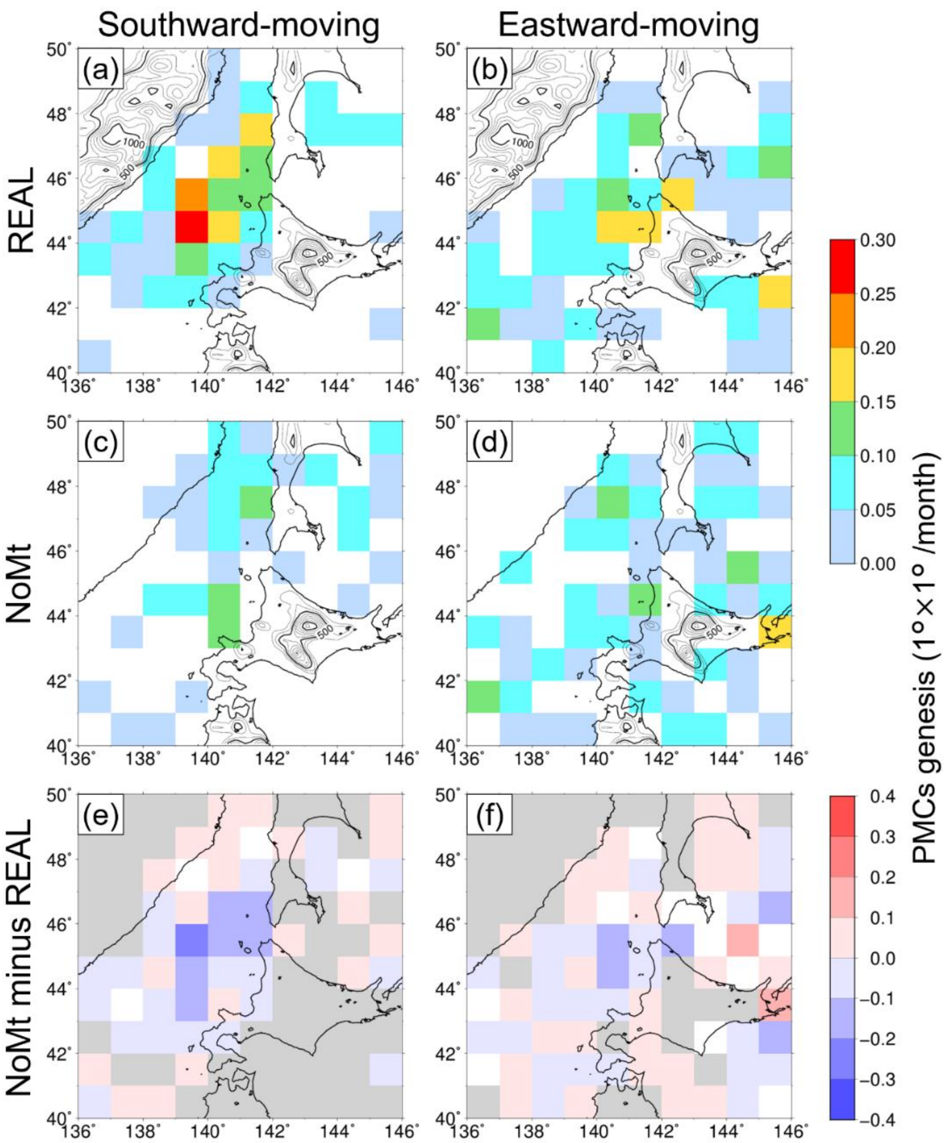


616

617 Fig. 6 Distribution of PMC genesis in January: (a) and (b) REAL experiment, (c) and (d) NoMt experiment, (e) and (f) difference (i.e., NoMt − REAL). Left (right) panels show southward (eastward)-moving PMCs.

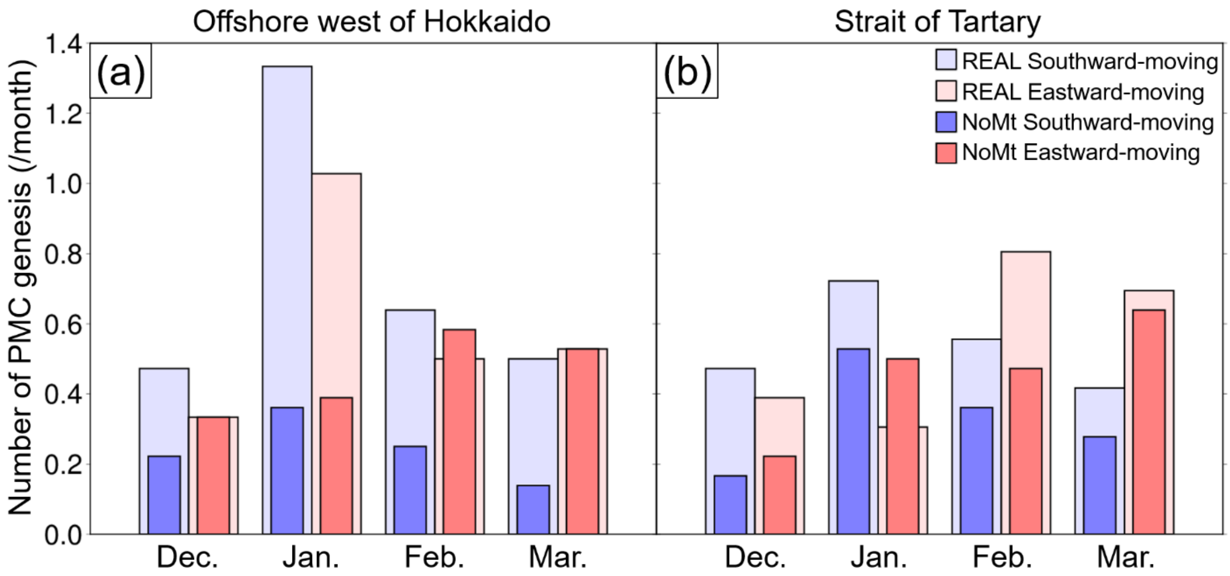


Fig. 7 Number of PMCs generated (a) in the offshore area west of Hokkaido (43°–46°N, 138°–142°E) and (b) in the Strait of Tartary (46°–49°N, 138°–142°E). Blue (red) bar indicates the number of southward (eastward)-moving PMC genesis. Light (dark) color indicates the REAL (NoMt) experiment.

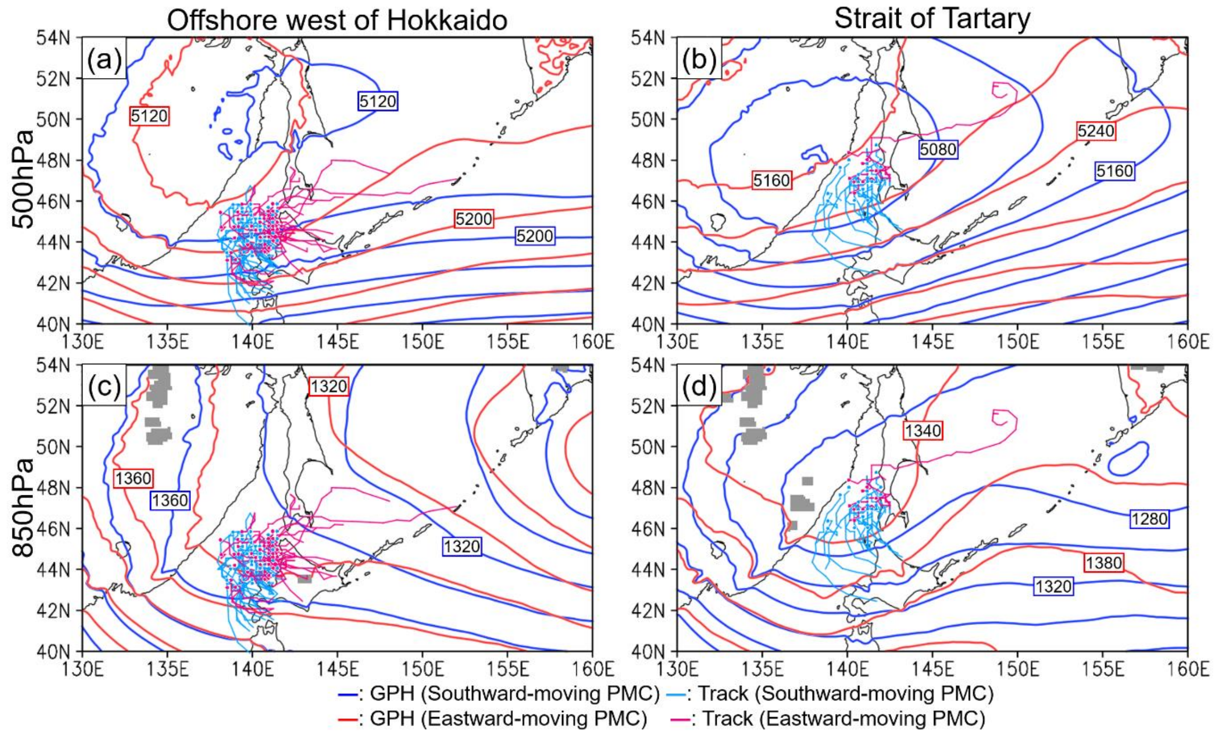


Fig. 8 Composite fields of geopotential height (contour; m) in REAL experiment at (a) and (b) 500 hPa and (c) and (d) 850 hPa. (a) and (c) offshore west of Hokkaido, (b) and (d) Strait of Tartary. Blue (red) contours indicate the geopotential height for southward (eastward)-moving PMCs. Colored dots and tracks indicate genesis location and track of PMCs (light blue: southward-moving PMCs, light red: eastward-moving PMCs), respectively.

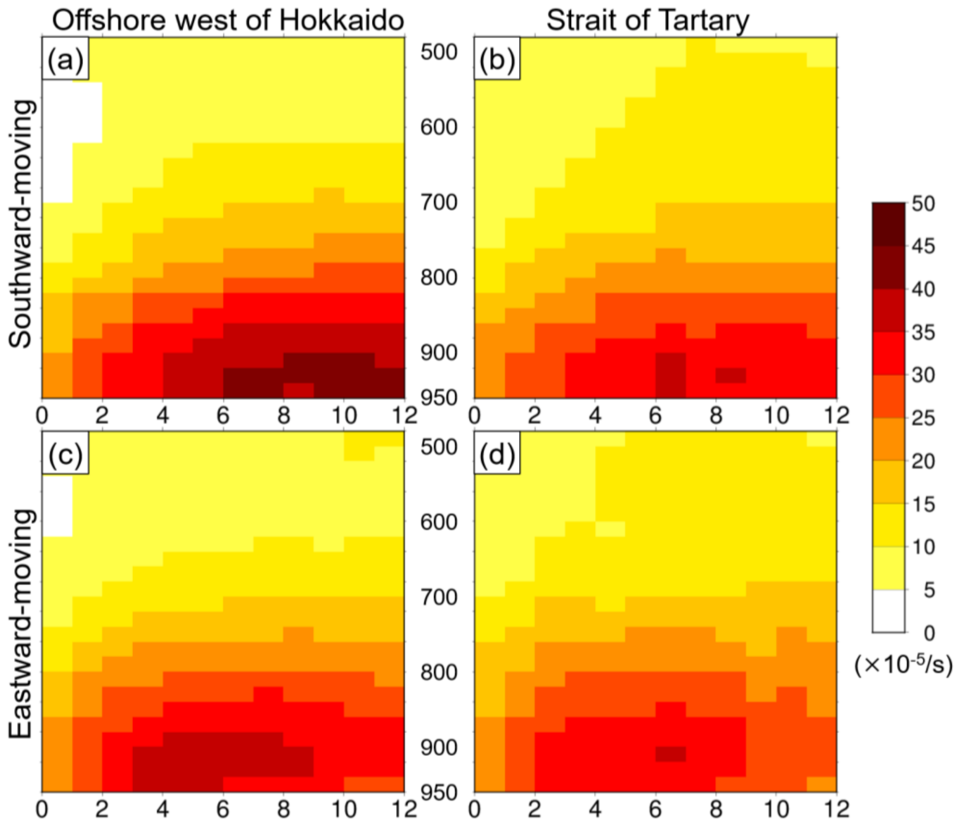


Fig. 9 Time series of the PMC's relative vorticity composited at each pressure height until 12 hours after the PMCs genesis: (a) and (c) PMCs generaged offshore west of Hokkaido, (b) and (d) Strait of Tartary. (a) and (b) for southward-moving PMCs and (c) and (d) for eastward-moving PMCs. The vorticity is averaged within the 60 km radius from the center of PMC.

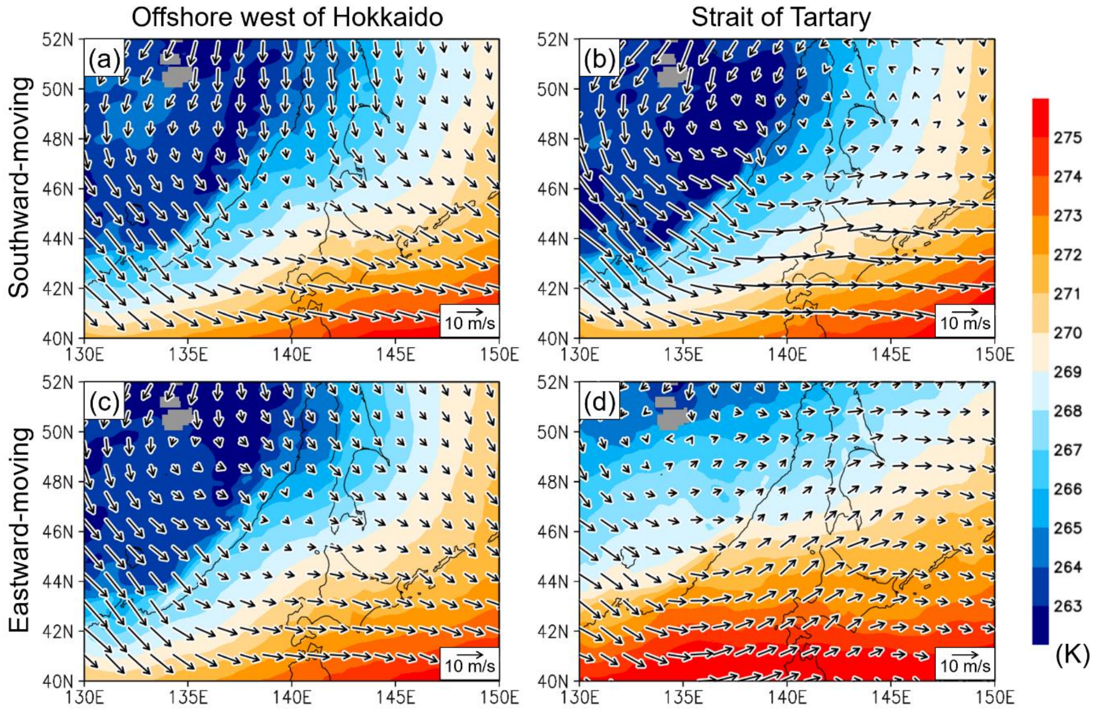


Fig. 10 Composite fields of potential temperature (shading; K) and horizontal winds (vectors) at 850 hPa for the 12 hours before PMC genesis: (a) and (c) offshore west of Hokkaido, (b) and (d) Strait of Tartary. (a) and (b) represent southward-moving PMCs and (c) and (d) represent eastward-moving PMCs.

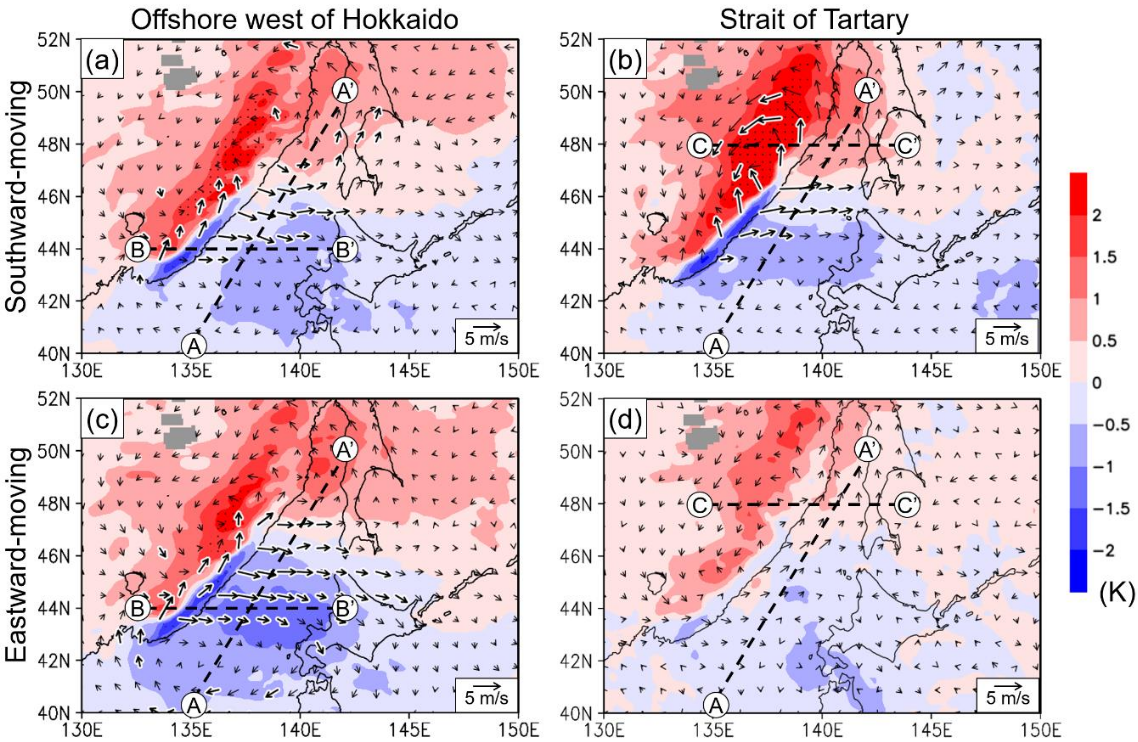


Fig. 11 Composite fields of the differences between REAL experiment and NoMt experiment (NoMt − REAL) in potential temperature (shading; K) and horizontal winds at 850 hPa (vector) for the 12 hours before PMC genesis: (a) and (c) offshore west of Hokkaido, (b) and (d) Strait of Tartary. (a) and (b) represent southward-moving PMCs and (c) and (d) represent eastward-moving PMCs. Dots and thick arrows indicate statistical significance at the 5% level for the difference between the experiments (Welch's t-test) Potential temperatures over the dash lines are shown in Fig. 12.

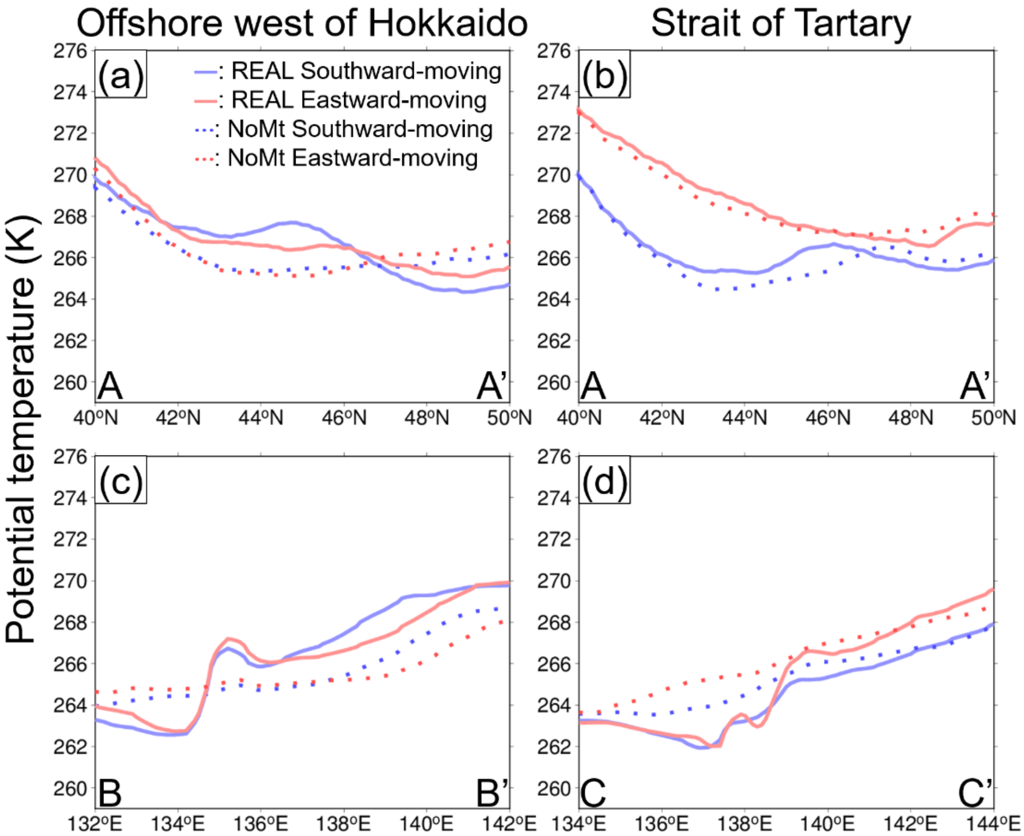


Fig. 12 Potential temperature (K) along the lines in Fig. 11: (a) and (b) A–A', (c) B–B', (d) C-C’. Solid (broken) lines indicate REAL (NoMt) experiment. Blue (red) color shows southward- (eastward-) moving PMCs.

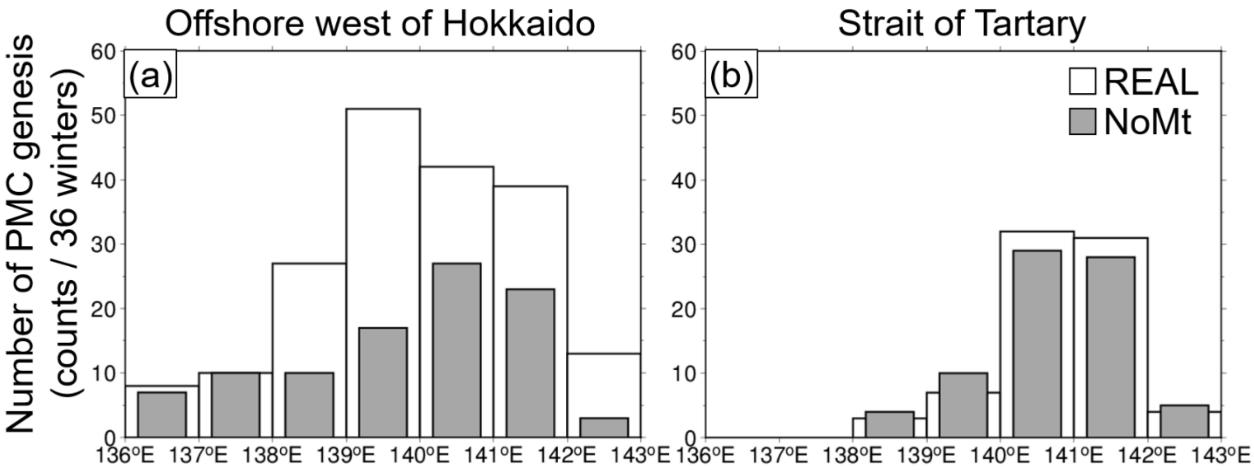


Fig. 13 Number of PMCs generated at each longitude. White (gray) bar indicates the REAL (NoMt) experiment. Numbers given here include PMCs whose lifespan was longer than six hours.

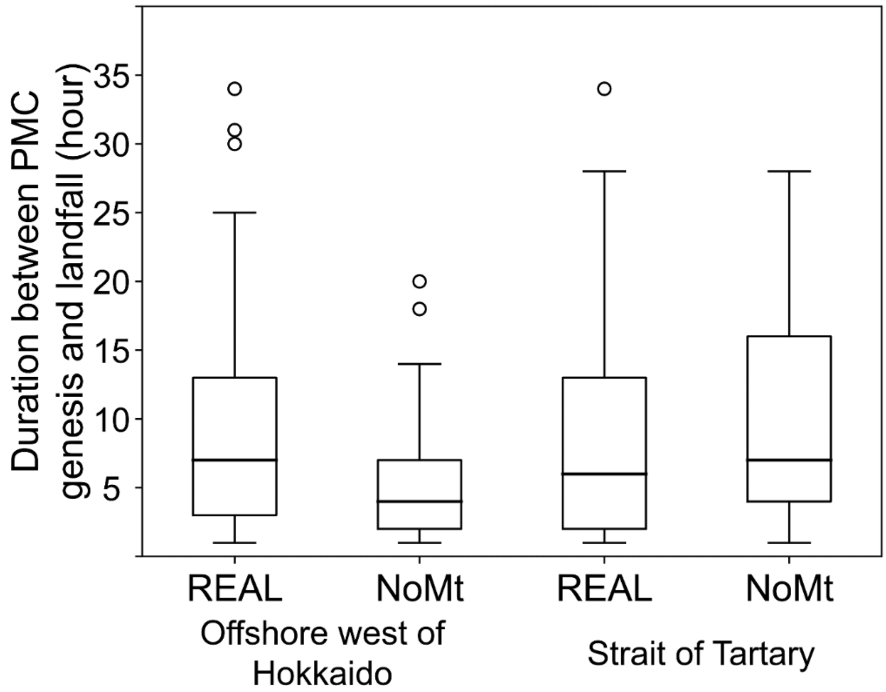


Fig. 14 Duration between PMC genesis and landfall. Results given here include PMCs whose lifespan is longer than six hours.

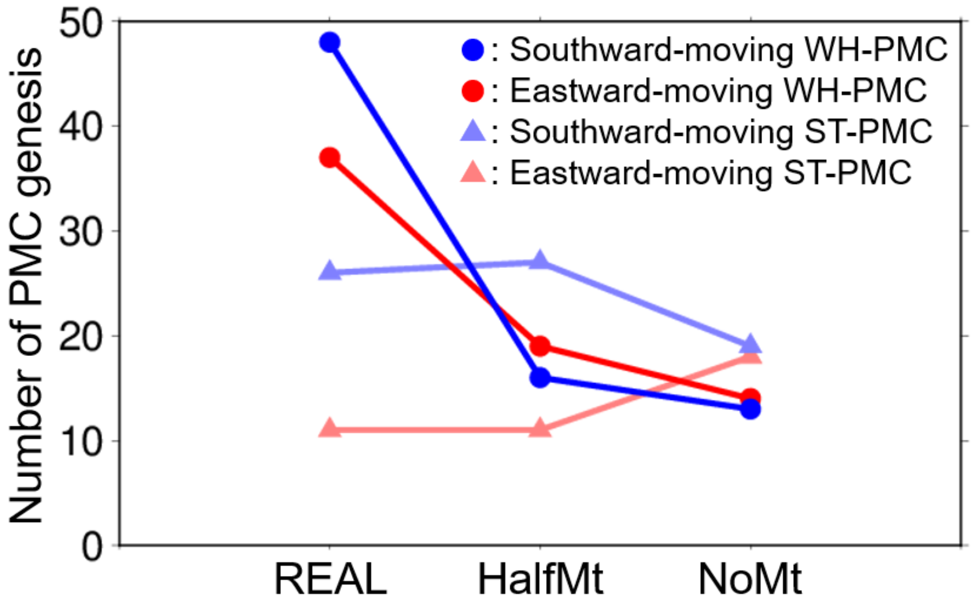


Fig. 15 Comparison of PMC genesis number within the analysis domain (43°–49°N, 138°–142°E) in January for three different mountain height setting. HalfMt experiment uses halved topography only for the Sikhote-Alin mountain range.

Table. 1 Comparison of PMCs between REAL experiment and NoMt experiment.

| Offshore west of Hokkaido (WH-PMCs) | REAL⇒NoMt |
|---|---|
| | Southward- and eastward-moving |
| Number of PMCs genesis | Decreased |
| Westerly wind from the continent | Intensified and become horizontally uniform |
| Horizontal wind shear (northerly－northwesterly) | Shifted to the north (from offshore west of Hokkaido to Strait of Tartary) |
| Zonal potential temperature gradient | Shifted to the east (from offshore west of Hokkaido to near the west coast of Hokkaido) |
| Meridional potential temperature gradient | Weakened |

| Strait of Tartary (ST-PMCs) | REAL⇒NoMt | |
|---|---|---|
| | Southward-moving | Eastward-moving |
| Number of PMCs genesis | Unchanged | Unchanged |
| Westerly wind from the continent | Intensified and become horizontally uniform | Unclear |
| Horizontal wind shear (northerly－northwesterly) | Slightly shifted to the north (Strait of Tartary) | Unclear |
| Zonal potential temperature gradient | Unclear | Unclear |
| Meridional potential temperature gradient | Shifted to the north (around 47°N to 48°N) | Unclear |